Supplement for: Atmospheric histories and emissions of chlorofluorocarbons CFC-13 ($CClF_3$), ΣCFC-114 ($C_2Cl_2F_4$), and CFC-115 (C_2ClF_5)

Martin K. Vollmer[1], Dickon Young[2], Cathy M. Trudinger[3], Jens Mühle[4], Stephan Henne[1], Matthew Rigby[2], Sunyoung Park[5], Shanlan Li[5], Myriam Guillevic[6], Blagoj Mitrevski[3], Christina M. Harth[4], Benjamin R. Miller[7,8], Stefan Reimann[1], Bo Yao[9], L. Paul Steele[3], Simon A. Wyss[1], Chris R. Lunder[10], Jgor Arduini[11,12], Archie McCulloch[2], Songhao Wu[5], Tae Siek Rhee[13], Ray H. J. Wang[14], Peter K. Salameh[4], Ove Hermansen[10], Matthias Hill[1], Ray L. Langenfelds[3], Diane Ivy[15], Simon O'Doherty[2], Paul B. Krummel[3], Michela Maione[11,12], David M. Etheridge[3], Lingxi Zhou[16], Paul J. Fraser[3], Ronald G. Prinn[15], Ray F. Weiss[4], and Peter G. Simmonds[2]

[1]Laboratory for Air Pollution and Environmental Technology, Empa, Swiss Federal Laboratories for Materials Science and Technology, Überlandstrasse 129, 8600 Dübendorf, Switzerland
[2]Atmospheric Chemistry Research Group, School of Chemistry, University of Bristol, Bristol, UK.
[3]Climate Science Centre, CSIRO Oceans and Atmosphere, Aspendale, Victoria, Australia.
[4]Scripps Institution of Oceanography, University of California at San Diego, La Jolla, California, USA.
[5]Kyungpook Institute of Oceanography, Kyungpook National University, South Korea.
[6]METAS, Federal Institute of Metrology, Lindenweg 50, Bern-Wabern, Switzerland.
[7]Earth System Research Laboratory, NOAA, Boulder, Colorado, USA.
[8]Cooperative Institute for Research in Environmental Sciences, University of Colorado, Boulder, Colorado, USA.
[9]Meteorological Observation Centre (MOC), China Meteorological Administration (CMA), Beijing, China.
[10]Norwegian Institute for Air Research, Kjeller, Norway.
[11]Department of Pure and Applied Sciences, University of Urbino, Urbino, Italy.
[12]Institute of Atmospheric Sciences and Climate, Italian National Research Council, Bologna, Italy.
[13]Korea Polar Research Institute, KIOST, Incheon, South Korea.
[14]School of Earth and Atmospheric Sciences, Georgia Institute of Technology, Atlanta, Georgia, USA.
[15]Center for Global Change Science, Massachusetts Institute of Technology, Cambridge, Massachusetts, USA.
[16]Chinese Academy of Meteorological Sciences (CAMS), China Meteorological Administration (CMA), Beijing, China.

Correspondence to: Martin K. Vollmer
(martin.vollmer@empa.ch)

S-1 Introduction

The supplement of this article consists of this text file and the following separate tables, saved as .csv files:

Table S1. Firn air measurements and firn model results

Table S2. Three sets of Cape Grim Air Archive measurements

Table S3. Assemblage of all archived canister air results for the Northern Hemisphere

Table S4. Assemblage of all archived canister air results for the Southern Hemisphere

Table S5. King Sejong (Antarctica) flask sample results

Table S6. Abundances derived from Bristol inversion.

Table S7. Emissions derived from Bristol inversion.

Table S8. Results from CSIRO inversion

Table S9. AFEAS bottom-up emission estimates

S-2 ΣCFC-114 Nomenclature

In this paper we adopt a nomenclature of ΣCFC-114 to denote the combined measurements of the symmetrical CFC-114 molecule (1,2-dichlorotetrafluoroethane, $CClF_2CClF_2$, CAS 76-14-2) and the asymmetrical CFC-114a molecule (1,1-dichlorotetrafluoroethane, CCl_2FCF_3, CAS 374-07-2). On the Medusa-GCMS instrumentation used in this study, these two isomers cannot be separated chromatographically and mass-spectrometrically.

S-3 Station Coverage

In Table S10 we provide a list of the station coverage for the data used in this analysis.

S-4 Measurements Details and Comparisons

S-4.1 Cape Grim Air Archive Measurements Used in this Study

The Cape Grim Air Archive (CGAA) has so far been analyzed three times on the CSIRO laboratory Medusa-GCMS (aspendale-medusa, Medusa-9) for halocarbons. Measurements were made by CSIRO staff in close collaboration with visiting scientist in 2006 (B. R. Miller), 2011 (D. Ivy), and 2016 (M. K. Vollmer). Minor CFC measurement results from these study periods are published here for the first time. The 2011 analysis did not include measurements of CFC-115. Some details for the individual study periods are given in Miller et al. (2010) and Ivy et al. (2012). Major changes between the three analysis sets were regarding chromatography columns and mass spectrometer (MS). For the 2006 analysis, a Porabond Q column was used (see main text "traditional" AGAGE Medusa setup), for 2011 a GasPro column was used (Ivy et al., 2012) and for 2016 an additional GasPro precolumn was fitted. Also, the 2016 analysis was based on 3 L samples and the MS amplifier settings were

Table S10. Station List and Data Used for CFC-13 ($CClF_3$), ΣCFC-114 ($C_2Cl_2F_4$), and CFC-115 (C_2ClF_5).[a]

Station	Network/ Institution	Lat °N	Lon °E	Altitude[b] (m.a.s.l.)	Instrument	Data availability [mm/yyyy] CFC-13	ΣCFC-114	CFC-115
Zeppelin	AGAGE	78.9	11.9	475	Medusa	09/2010 – 12/2016	09/2010 – 12/2016	09/2010 – 12/2016
NEEM[c]	see c)	77.5	-51.1	2484	Medusa flask	firn air		
Mace Head	AGAGE	53.3	-9.9	5	Medusa	11/2003 – 12/2016	11/2003 – 12/2016	11/2003 – 12/2016
Tacolneston	UK DECC / regional	52.5	1.1	69	Medusa	12/2008 – 12/2016	12/2008 – 12/2016	12/2008 – 12/2016
Dübendorf	AGAGE / urban	47.4	8.6	432	Medusa	–	–	–
Jungfraujoch	AGAGE	46.5	8.0	3580	Medusa	04/2008 – 12/2016	04/2008 – 12/2016	10/2009 – 12/2016
Monte Cimone	AGAGE	44.2	10.7	2165	GCMS	–	07/2007 – 12/2016	07/2007 – 12/2016
Trinidad Head	AGAGE	41.0	-124.1	107	Medusa	03/2005 – 12/2016	03/2005 – 12/2016	03/2005 – 12/2016
Shangdianzi	AGAGE	40.7	117.1	293	Medusa	05/2010 – 12/2016	05/2010 – 12/2016	05/2010 – 12/2016
North. Hem. sites	SIO and others	–		–	Medusa flasks		10/1973 – 12/2013	
Gosan	AGAGE	33.3	126.2	72	Medusa	11/2007 – 12/2016	05/2008 – 12/2016	11/2007 – 12/2016
La Jolla	AGAGE / urban	32.9	-117.3	10	Medusa	–	–	–
Ragged Point	AGAGE	13.2	-59.4	15	Medusa	05/2005 – 12/2016	05/2005 – 12/2016	05/2005 – 12/2016
Cape Matatula	AGAGE	-14.2	-170.6	42	Medusa	05/2006 – 12/2016	05/2006 – 12/2016	05/2006 – 12/2016
Aspendale	AGAGE / urban	-38.0	145.1	10	Medusa	–	–	–
Cape Grim	AGAGE	-40.7	144.7	94	Medusa	01/2004 – 12/2016	01/2004 – 12/2016	01/2004 – 12/2016
Cape Grim CGAA	CSIRO/BoM	-40.7	144.7	94	Medusa flasks		04/1978 – 12/2010	
King Sejong	KOPRI/Empa	-62.2	-58.8	2	Medusa flasks	02/2007 – 12/2014	02/2007 – 12/2014	02/2007 – 12/2014
Law Dome DSSW20K	see d)	-66.7	112.5	1200	Medusa flask	firn air		
South Pole		-90.0	-4.8	2810	Medusa flask	firn air		

a) Stations are listed in latitudinal order from north to south. Data availability for in situ and flask records with start and end dates. Active AGAGE sites are updated to 2016. Older GCMS results from an ADS (Adsorption Desorption System) preconcentration unit are not listed here and not used in the analysis. Major gaps in data are (in yymm): Zeppelin: CFC-13: 1207–1302, ΣCFC-114: 1207–1405, 1411–1604, CFC-115: 1510–1603. Mace Head: CFC-13: 0610–0705, ΣCFC-114: 0501–0906, CFC-115: 0707–0712. Jungfraujoch: ΣCFC-114: 1403–1501. Monte Cimone: ΣCFC-114 and CFC-115 data prior to 0707 considered unreliable for this analysis. Shangdianzi: not operational for 1209–1512. ΣCFC-114: data not used due to potential mass spectrometer interference. Gosan: all three compounds: 1611-1704. Ragged Point: CFC-13: 0701–0707, ΣCFC-114: 1407–1503. Cape Grim: CFC-13: 0610–0710, 0802–0902. Stations Dubendorf (Switzerland), La Jolla (California), and Aspendale (Australia) denoted as "urban" are institute-based Medusas in urban areas with primary purposes other than collecting clean background air. Their ambient air measurements can therefore be intermittent. Tacolneston (England, UK DECC network) has large urban centers in its footprints. These stations were used only for qualitative assessment in this analysis.
Abbreviations are:
AGAGE: Advanced Global Atmospheric Gases Experiment.
SIO: Scripps Institution of Oceanography.
CSIRO/BoM: CSIRO Oceans and Atmosphere / Australian Bureau of Meteorology.
KOPRI: Korea Polar Research Institute.
Empa: Swiss Federal Laboratories for Materials Science and Technology.
DECC: Department of Energy and Climate Change.
NILU: Norwegian Institute for Air Research.
b) These are the altitudes of the science buildings. Air intake altitudes at some stations may be higher.
c) NEEM: North Greenland Eemian Ice Drilling (University of Copenhagen/NEEM consortium/CSIRO).
d) Law Dome: operated by Australian Antarctic Program/CSIRO.

increased to enhance detector sensitivity and improved integrations of small peaks. Further, in 2015 the Agilent MSD 5973 was replaced by a Agilent MSD 5975. For the present study we have chosen to use averaged results where multiple analyses are

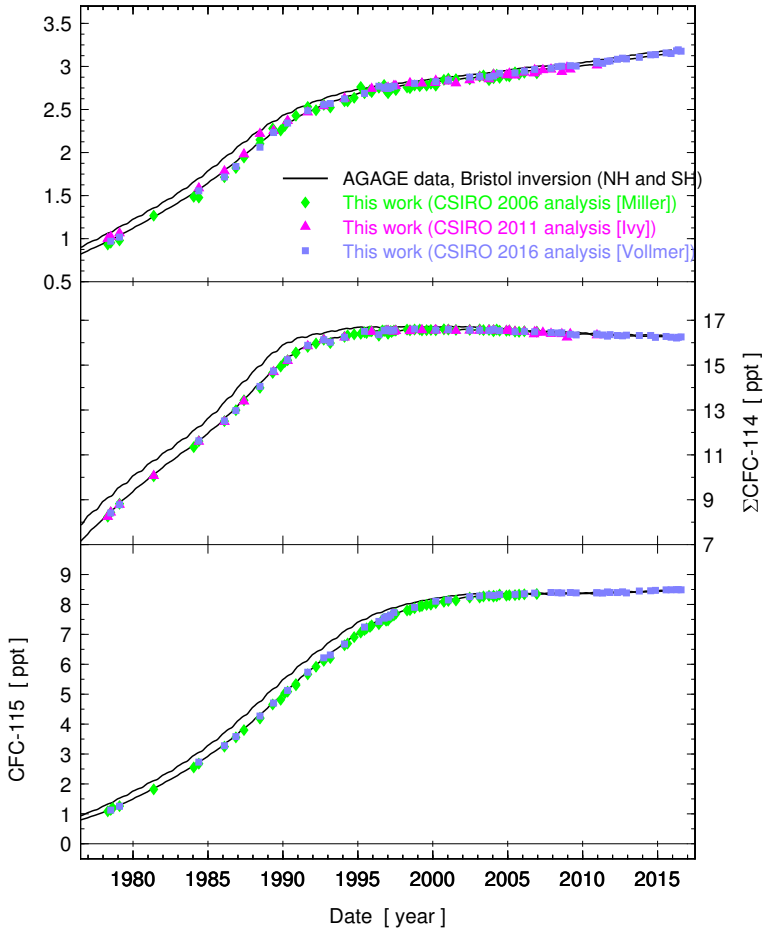

Figure S1. Comparison of the measurements of CFC-13, ΣCFC-114, and CFC-115 in the Cape Grim Air Archive (CGAA) from three sets of previously unpublished measurements conducted during three measurement periods.

available for individual samples. A comparison of the three data sets is shown in Fig. S1 and shows generally good agreement. Some deviations exist for the early record of CFC-13. All CGAA measurement results are listed in Table S2.

S-4.2 Comparison With CGAA Measurements by Oram (1999)

Subsamples of 10 of the same Cape Grim Air Archive (CGAA) samples were analyzed by both Oram (1999) and in the present study (composite of the 3 analysis sets). This allows for a direct comparison of the measurements and an assessment of calibration scale differences (Fig. S2). CFC-13 Measurements by Oram (1999) are reported on the UEA calibration scale and those for CFC-114, CFC-114a and CFC-115 on a UEA-preliminary calibration scale. The results of the present study are reported on the METAS-2017 calibration scale for CFC-13 and on the SIO-05 calibration scales for ΣCFC-114 and CFC-115.

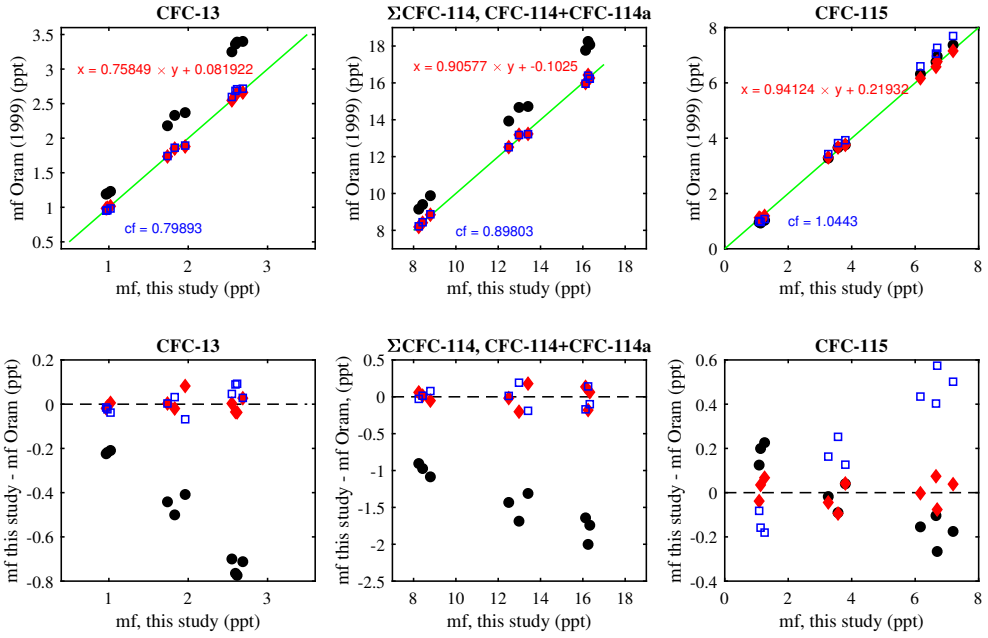

Figure S2. Comparison of CGAA subsamples analyzed for this study and by Oram (1999). The original results are shown as mole fractions (mf) as black filled circles in the upper row. To convert to our calibration scales, two types of conversions were tested and applied to the Oram (1999) results, a linear conversion without offset/constant term (in blue open squares) and one with an offset/constant term (red filled diamonds). Subplots in the lower row show mole fraction deviations before and after the conversions with the same color coding. The values from Oram are the numerical sum of the individually measured CFC-114 and CFC-114a while results of ΣCFC-114 from the present study are from measurements of un-separated isomers.

CFC-13 mole fractions for the same subsamples are generally higher in Oram (1999) than those in our study. A conversion factor for UEA to METAS-2017 of 0.798 is calculated from the mean of the samples' ratios (Fig. S2). For the conversion of the numerical sum of CFC-114 and CFC-114a from Oram (1999) to ΣCFC-114 from the present study, the factor is 0.898. However, newer UEA calibration scales (UEA-2014) for CFC-114 and CFC-114a were established by Laube et al. (2016) along with a re-analysis of the CGAA samples (see Section S-4.4). For CFC-115, a conversion based on the mean of the measurement ratios (1.045) appears inappropriate because the extrapolation of the linear fit through the two data sets deviates strongly from origin. A conversion of the form 0.9430×y + 0.2176 applied to the Oram (1999) data (as y in ppt) results in overall smaller absolute deviations.

S-4.3 Comparison With Study by Sturrock et al. (2002)

The purpose of this section is to provide the numerical firn air results used in Sturrock et al. (2002) (they were not numerically published in that study) and to illustrate the CFC-115 discrepancy of that study with the present one in more detail. This was

Table S11. W20K firn air results of Sturrock et al. (2002). These results are from measurements on an ADS-GCMS. The results are reported on the interim UB98B calibration scale. Precisions are the standard deviations (1 σ) of the means.

Sample	Depth	ΣCFC-114			CFC-115		
UAN number	[m]	Age	ppt	precision [ppt]	Age	ppt	precision [ppt]
UAN980142	29.0	1989.57	15.64	0.17	1992.20	5.86	0.05
UAN980144	41.7	1983.89	11.76	0.03	1985.27	3.35	0.10
UAN980145	44.5	1977.21	7.68	0.04	1978.10	1.63	0.12
UAN980146	47.0	1964.65	1.68	0.02	1970.38	0.00	0.00
UAN980147	49.5	1955.63	0.00	—	1949.08	0.00	0.00
UAN980149	52.0	1934.23	0.00	—	1935.09	0.00	0.00
UAN980150	52.0	1934.23	0.00	—	1935.09	0.00	0.00

stimulated by a hypothesis that the discrepancy may have also been caused by calibration scale discrepancies, in addition to the omission of an upward gas flow in the firn, as outlined by Trudinger et al. (2013).

The Antarctic W20K measurements from Sturrock et al. (2002) are given in Table S11. These are reported in the AGAGE "interim" UB-98B calibration scales. Using results from measurements of subsamples of the same parent samples, and reported on the SIO-05 calibration scales, our ΣCFC-114 results are 3–5% lower, and our CFC-115 results 1–4% higher compared to the Sturrock et al. (2002) reconstructed mole fraction history. This discrepancy is in relatively good agreement with the independently determined SIO-05/UB-98B conversion factors of 0.9565 for ΣCFC-114 and 1.0177 for CFC-115 (see main text), with which the Sturrock et al. (2002) data need to be multiplied to report them on the SIO-05 calibration scales.

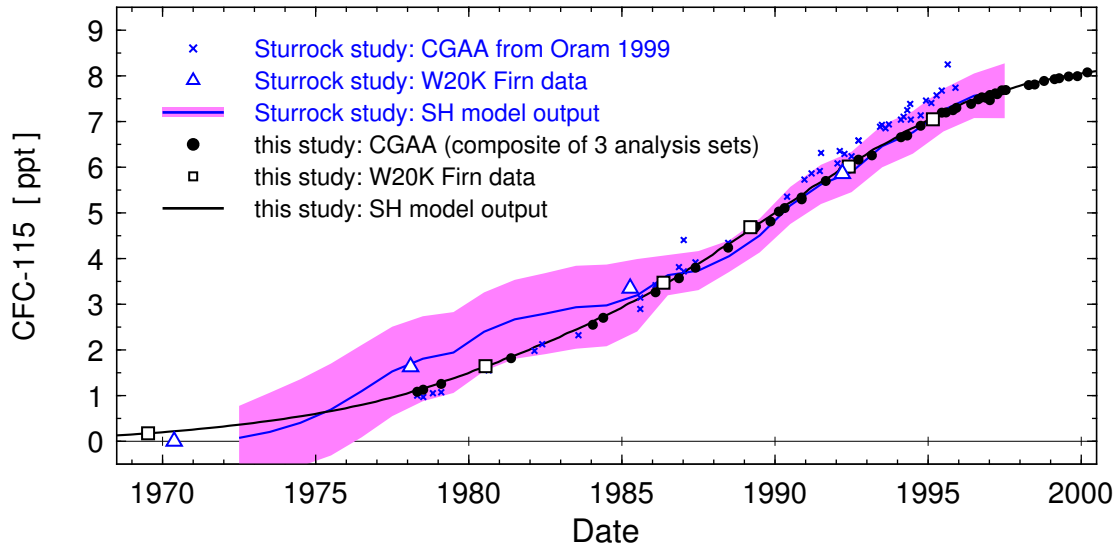

Figure S3. Comparison of CFC-115 results by Sturrock et al. (2002) with the present study. See text for details.

The graphical comparison of the Sturrock et al. (2002) results with the present study is shown in Fig. S3. Note that our results are reported on the SIO-05 calibration scales and the Sturrock et al. (2002) results are reported on the UB-98B calibration scale. Sturrock et al. (2002) had to convert the CGAA data from Oram (1999) to UB-98B by using a conversion factor of 0.96 for CFC-115, a factor that was determined from a comparison of modern UEA and AGAGE data (Sturrock et al., 2002). However, as shown in section S-4.2, a conversion of UEA to AGAGE data using a constant is not appropriate. Nevertheless, the errors in the various conversion factors are relatively small and not the main cause of the discrepancy in the early part of the records between the Sturrock et al. (2002) results and those from our study. The discrepancy is predominantly caused by the age-determination for the firn air samples, which has been revised for the present study using a newer version of the CSIRO firn model that includes the previously-neglected upward flow of air in the firn due to pore compression (see Trudinger et al. (2013) for more detail).

S-4.4 On the CFC-114 and CFC-114a Isomers

The Medusa-GCMS measurement technology used in AGAGE does not allow for the analytic separation of CFC-114 ($CClF_2CClF_2$) from its isomer CFC-114a (CCl_2FCF_3). To account for this, we have adopted the terminology of ΣCFC-114 throughout this study, to denote the combined measurement of the two isomers. This deficiency also prevents us from constructing deconvoluted atmospheric histories for the two isomers. The purpose of this section is to assess potential biases introduced with this deficiency with respect to the single-isomer measurements, in particular related to the (for our instruments hypothetical) numeric sum of the individual mole fractions of the two separated isomer measurements ($CFC\text{-}114_{sum}$ = CFC-114 + CFC-114a). We also provide a comparison of CGAA measurements made for ΣCFC-114 using Medusa-GCMS technology (on the SIO-05 calibration scale) with CFC-114 and CFC-114a measurements made by the University of East Anglia (UEA), which used a measurement technology that can separate the two isomers, and which were reported on the UEA-2014 calibration scales (Laube et al., 2016). This comparison will illustrate the isomer issue and add at understanding to what extent the SIO and UEA calibration scales can be compared.

The main point is that ΣCFC-114 does potentially not equal $CFC\text{-}114_{sum}$ because of a combination of two effects. Firstly the per-mol sensitivities of the mass spectrometer (MS) are likely to differ for the two isomers. For the UEA measurements it was shown for m/z 135, that the MS exhibited a per-mol sensitivity for CFC-114a that was 2.3 times that of CFC-114 (online discussion to Laube et al. (2016)). For our Medusa-GCMSs, We do not know these relative molar sensitivities. If they were identical for the two isomers, than ΣCFC-114 = $CFC\text{-}114_{sum}$. However, below we assume that CFC-114a is also more sensitive on the Medusa-GCMSs, as it is on the UEA instrument. Secondly the analysis by Laube et al. (2016) revealed a time-variable CFC-114a fraction in the atmosphere, where CFC-114a/$CFC\text{-}114_{sum}$ in the CGAA ranged from 4.1% (samples collected in 1978) to 6.5% (samples collected in 2014) as is shown in Fig. S4a. Note that Laube et al. (2016) reported relative CFC-114a/CFC-114 ratio while we report CFC-114a/$CFC\text{-}114_{sum}$, hence the numbers shown here deviate slightly from the numbers in the text and figures of their publication.

A first consideration is one of absolute calibration. In this context it is important to know that the SIO primary standards made for ΣCFC-114 are synthetically produced from pure reagent and diluted in synthetic air, hence their isomer composition

is that of the pure reference material. All subsequent lower-hierarchy standards (secondary, tertiary, quarternary) are whole air fillings of relatively clean background air, hence their isomer composition is that of ambient air at the times of their fillings.

The SIO-05 calibration scale for ΣCFC-114 is based on commercially obtained seemingly high-purity CFC-114 (1,2-dichlorotetrafluoroethane, Aldrich Chemical Co.; Product No. 29524-8; Lot No. 07408MU; November 1999). However, results shown below demonstrate that the stated 99.9% purity (by gas liquid chromatography) by the manufacturer does not include isomeric impurities of CFC-114a in CFC-114. To assess the CFC-114a fraction in the commercial sample, an aliquot of the primary standard P-037, which was made from this sample, was analyzed for CFC-114a and CFC-114 at UEA. Results communicated to SIO in December 2008 (CFC-114 = 19.7 ppt, CFC-114a = 1.40 ppt) were based on preliminary calibration scales (presumably the same as used by Oram (1999)). We convert these to UEA-2014 calibration scales using the conversion factors from Laube et al. (2016) yielding CFC-114 = 18.09 ppt and CFC-114a = 0.987 ppt (conversions of exemplary numbers for Cape Grim, also provided in the same communication, agree well with those recently published by Laube et al. (2016), giving confidence in this procedure). Thus CFC-114a/CFC-114_{sum} in the reference material, used to produce the SIO-05 calibration scale, corresponds to 5.2%. As a note on the side, the pure reference material used by Laube et al. (2016) to produce the UEA-2014 calibration scales, contained 5.7% CFC-114a (unclear if ratioed to CFC-114 or to CFC-114_{sum}), hence containing a surprisingly similar fraction of CFC-114a compared to the pure reagent used to produce the SIO-05 calibration scale. CFC-114_{sum} in the P-037 aliquot is then 19.08 ppt on the UEA-2014 calibration scale and compares with the SIO-05 assignment for ΣCFC-114 of 19.24 ppt in P-037. This 0.8% difference could derive from measurement uncertainties, uncertainties in the calibration scales of both institutions, a result of unaccounted-for potentially differing molar sensitivities for the isomers on the Medusa-GCMS, or a combination of all these.

If all air samples (and all whole-air lower-ranking standards) had a constant CFC-114a/CFC-114_{sum} (that differed from that of the primary standards), then a bias of ΣCFC-114 vs. CFC-114_{sum} would be introduced in the AGAGE measurements. However such a bias would affect all measurements in the same way and the bias would be part of the in-accuracy of the primary calibration scale. It would however not create a bias among AGAGE measurement results. In reality though, CFC-114a/CFC-114_{sum} changed over time (Fig. S4a). The best example to demonstrate the difference between ΣCFC-114 and CFC-114_{sum} is the CGAA with air samples spanning over several decades of time-variable CFC-114a/CFC-114_{sum} (Figs. S4b and c).

There is an apparent complication in the conversion of ΣCFC-114 to CFC-114_{sum} for the CGAA (and for any air samples) measured on the Medusa-GCMSs. The link between the primary standards and the "endmember" air samples (ambient or stored in containers) is given by a hierarchy of whole air standards (most of which with a relatively modern, 2000–present, CFC-114a/CFC-114_{sum}). While it appears that their CFC-114a/CFC-114_{sum} is important in this exercise, these are ultimately canceling out such that we can conduct these calculations based on a single CFC-114a/CFC-114_{sum} reference assumption. For this we use the CFC-114a/CFC-114_{sum} of the primary standards (5.2%) as outlined above.

In Fig. S4b we also compare our CGAA record with CFC-114_{sum} from Laube et al. (2016). For the more recent part of the CGAA record CFC-114_{sum} is ∼2.5% lower compared to our ΣCFC-114, while the older parts of the two records agree better (also in percentage). This is suggestive of a nonlinear conversion for the UEA-2014 to SIO-05 calibration scales. However after conversion from ΣCFC-114 to CFC-114_{sum}, our CGAA record agrees more closely with that from Laube et al. (2016)

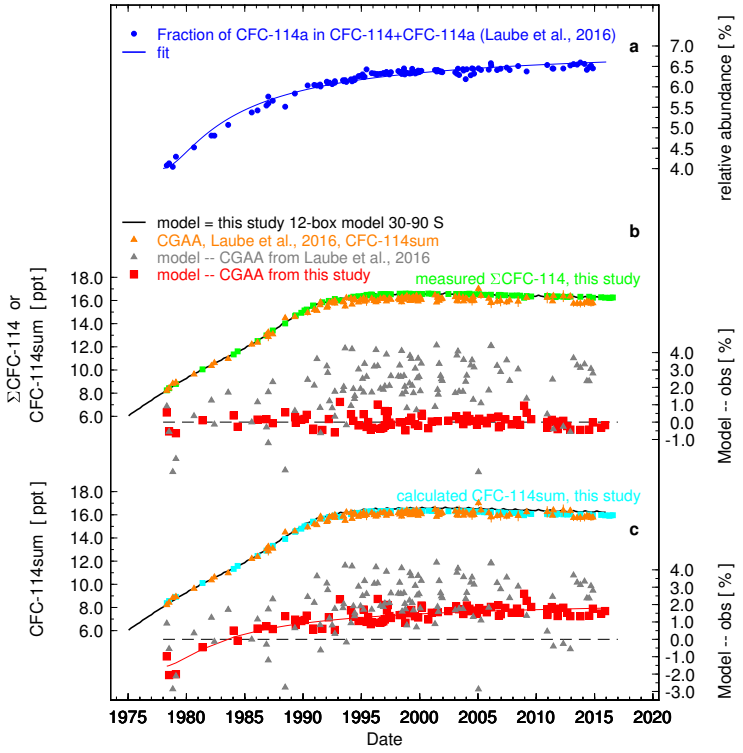

Figure S4. Cape Grim Air Archive (CGAA) measurements for ΣCFC-114 from this study with results from Laube et al. (2016). ΣCFC-114 is the combined measurement of the analytically non-separable CFC-114 and CFC-114a isomers on the Medusa-GCMS where as CFC-114_{sum} is the numeric sum of the individual CFC-114 and CFC-114a measurements. The relative fraction CFC-114a/CFC-114_{sum} (in percent) in Cape Grim Air Archive (CGAA) is shown in panel a (Laube et al., 2016). In panel b we show CGAA records of ΣCFC-114 (this study, in green) and CFC-114_{sum} (Laube et al., 2016) (in orange) and their deviations from our 12-box model results (red squares and gray triangles, respectively). In panel c, an exemplary conversion of our ΣCFC-114 measurements to CFC-114_{sum} is shown (in cyan) for our Medusa-GCMS measurements. This conversion is based on the CFC-114a/CFC-114_{sum} from panel a, a reference CFC-114a/CFC-114_{sum} of 5.2% in our primary standards, and the assumption that the molar sensitivity of CFC-114a in our mass spectrometer is 2.3 times that of CFC-114. This hypothetical Medusa-GCMS CFC-114_{sum} deviates from our 12-box model results similar to the deviations we calculate for the CGAA records from Laube et al. (2016). The results could indicate that some of the apparent differences between the CGAA records of this study and that published by Laube et al. (2016) derive from the unseparated isomers measurements. See text for details.

as is shown by the similar differences to the original 12-box model results (Fig. S4c). While this may be coincidental, it is intriguing that the nonlinear differences between the two records largely disappear with this conversion.

To summarize this section, if we assumed that the Medusa-GCMSs had a molar CFC-114a sensitivity that was 2.3 times that for CFC-114, and if the primary standards used to define the SIO-05 calibration scale had a CFC-114a/CFC-114 of 5.2%, which is likely fairly accurate, then our modern air sample ΣCFC-114 would need to be lowered by 1.8% to convert to CFC-114_{sum}. Such a conversion would reduce the current differences between our and the UEA CGAA results and remove most of the nonlinearity in this difference.

S-4.5 Antarctic Samples from King Sejong

With only the Cape Grim and Cape Matatula (American Samoa) stations, the AGAGE network is sparsely represented in the Southern Hemisphere. For this reason, regular flask samples have been collected since 2007 from King Sejong, Antarctica, thereby representing the most southern Medusa-GCMS based measurements. The South Korean station King Sejong (King George Island, South Shetland Islands) is maintained by the Korea Polar Research Institute (KOPRI). Weekly samples are filled with a metal-bellows or Teflon-coated neoprene membrane pump into internally electropolished stainless steel canisters. Yearly batches of canisters are analyzed on Medusa-GCMS instruments. The 2007 batch was measured on the Jungfraujoch Medusa-GCMS, the 2008 and 2009 batches on the Zeppelin Medusa-GCMS while under operation at Empa after construction, and all batches thereafter on the Medusa-GCMS in the Empa laboratory. Measurements were made against working standards which were ultimately referenced against the same primary references as the on-site measurements. The early measurements of 2007 and 2008 are deemed less reliable for the three CFCs and hence they were removed from this analysis. Numeric results of the King Sejong results are given in the separate Supplement Table S5. The results are shown in Fig. S5 along with Cape Grim and Jungfraujoch in-situ Medusa-GCMS measurements.

S-4.6 ΣCFC-114 Interferences in Polluted Air

ΣCFC-114 measurements on some of the Medusa-GCMS systems have shown artificial depletion of this compound in strongly polluted air masses. This has so far mainly been observed for the measurements at urban Dubendorf (Zurich, Switzerland), and Shangdianzi. An example is shown in Fig. S6. The depletion is speculated to originate from an interference in the mass spectrometer (MS) when large amounts of n-butane are present and measured, a compound that co-elutes with ΣCFC-114 on these two instruments. Details of this suppression mechanism are unclear but investigations are ongoing. It is not clear if the interference is equally strong for when n-butane is present but its ions not acquired in the analysis (n-butane is currently not measured at most AGAGE stations). For the example shown in Fig. S6 there is a strong anti-correlation between the two compounds, with a reduction in ΣCFC-114 by 0.20 ppt for an increase in n-butane of 1.0 ppb. We use this example for the quantification of the "interference uncertainty" discussed in the paper. Assuming that n-butane in background air is maximally 0.5 ppb, a depletion of 0.1 ppt of ΣCFC-114 would potentially result, which is on the order of 0.6 % for present-day ΣCFC-114 mole fractions. We use this estimate in the main text along with other uncertainties for ΣCFC-114 for the calculations of the total ΣCFC-114 uncertainties. We expect this to be an upper limit of an interference for the background stations. On the GasPro

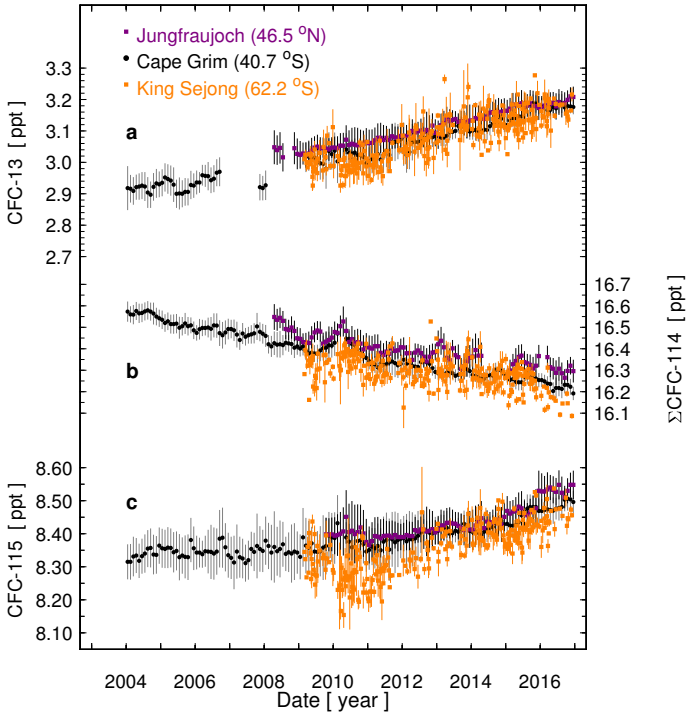

Figure S5. Measurement of the minor chlorofluorocarbons CFC-13 (a), ΣCFC-114 (b), and CFC-115 (c) from flask samples collected at the Korean Antarctic Station King Sejong. Results are shown along with monthly mean and std dev (1 σ) from pollution-filtered in-situ measurements at Cape Grim and Jungfraujoch.

chromatography columns used to measure the CGAA in 2011 and 2016, n-butane does not co-elute with ΣCFC-114 and hence we conclude that such interference is not present in these archived air measurements.

S-4.7 High-Resolution Records from Field and Urban Sites

High-resolution (2-hourly) records for the field and urban stations are shown in Fig. S7 for CFC-13, in Fig. S8 for ΣCFC-114, and in Fig. S9 for CFC-115. The purpose of these graphical displays is to present a qualitative overview of the presence and/or absence of pollution events at the sites. For the urban stations, the presence of pollution events is generally not very informative as nearby sources can easily obscure the existing situation within the footprint of the station. In particular for these low-temperature refrigerants, nearby sources are likely present and may be due to the research environment and institutions (e.g. ice core research), where these urban sites sample air from. However the absence of pollution events at an urban site is potentially a powerful and very informative result as it demonstrates that for the footprint of a normally highly emissive environment, no significant sources are present.

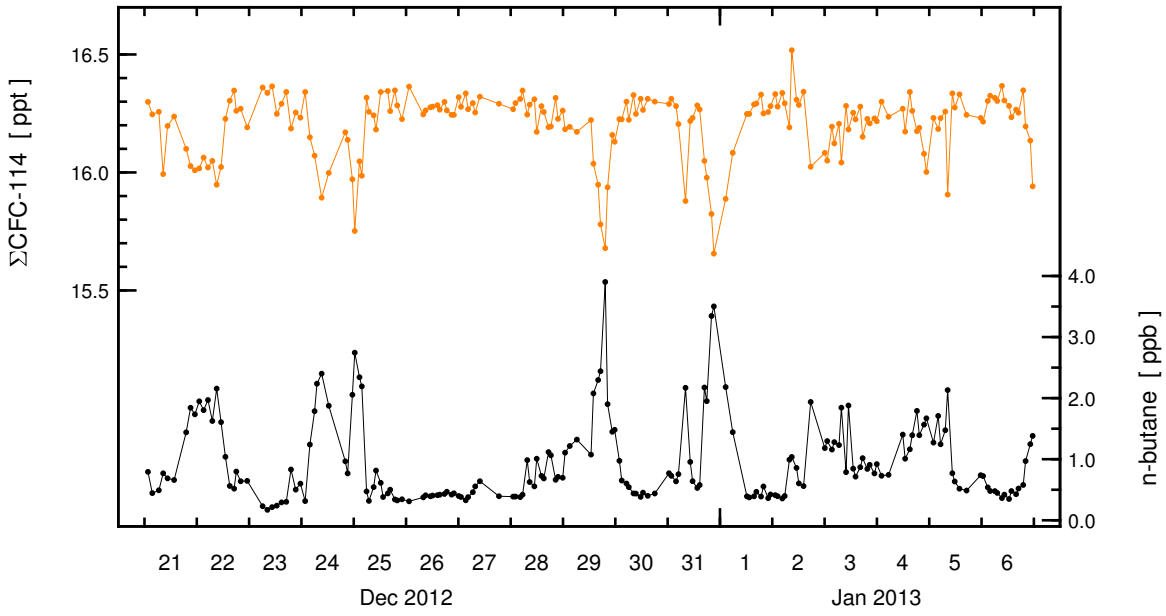

Figure S6. Medusa-GC quadrupole mass spectrometer interference for the co-eluting ΣCFC-114/n-butane shown for a ∼2-week period of urban air measured at Dübendorf (Zurich, Switzerland) using the Dübendorf Medusa-GCMS (Medusa-20). The ΣCFC-114 signal is suppressed when n-butane is present at elevated mole fractions. Suppression is 0.20 ppt ΣCFC-114 for an enhancement of 1.0 ppb n-butane.

S-5 Emissions Inventories for ΣCFC-114 and CFC-115

In the present study we use bottom-up emission estimates based on the Alternative Fluorocarbon Environmental Acceptability Study (AFEAS) as a prior in our inversion. AFEAS data are available on the AGAGE internet site at https://agage.mit.edu/data/afeas-data but values for CFCs were not calculated after 2003 because the AFEAS share of global CFC-11 and CFC-12 production was estimated to be approximately only 20% of the global amount. Apparently at that time, there was no production of CFCs-114 and 115 outside of the companies responding to AFEAS but a small tail of production was assumed in Table S9 in order to cater for any residual basic domestic needs in Article 5 countries.

Emissions were calculated from data on production and sales (divided among categories of use having different emission patterns). These data were compiled using reports from chemical producers, originally by the Chemical Manufacturers Association (1930 onward) and then, from 1990 onward, by AFEAS. Emissions occur throughout the world, with 85% to 90% arising in countries where production is reported (McCulloch et al., 1994). However, the evidence is that the remaining 10% to 15% of global demand was met by exports from reporting countries and that production of ΣCFC-114 and CFC-115 by producers that did not report to the AFEAS database was insignificant, so that the values given here are assumed to be global.

Prompt emissions from "short term" categories (aerosols and open cell plastic foams) occur within two years of production, so that half of the emission is in the year of production and half in the subsequent year. In the historical database, "fugitive"

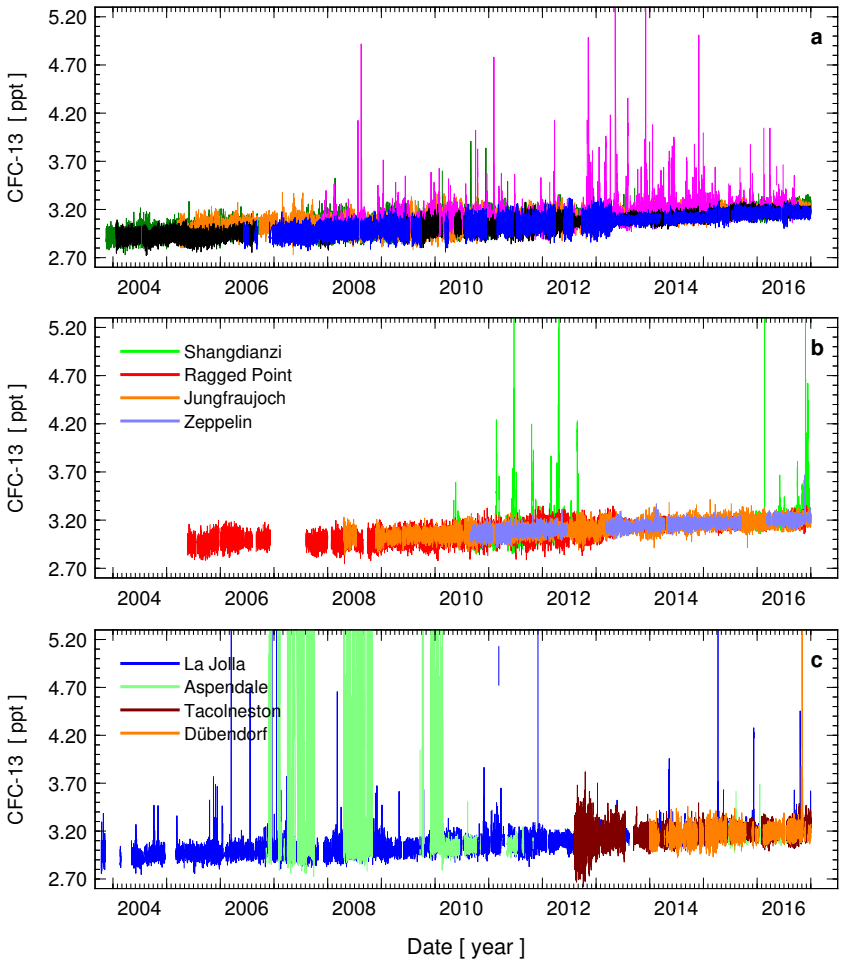

Figure S7. High-resolution (2-hourly) data sets for CFC-13 for nine field (panels a and b) and 4 urban sites (panel c). Gosan and Shangdianzi are the only field sites with significant pollution events recorded. CFC-13 is not measured at Monte Cimone. The urban sites show a general absence of pollution events except for La Jolla and for an early part of the Aspendale record, when leakage of CFC-13 cooling equipment in the institute building affected the air measurements. The reduction in the variability at e.g. Cape Matatula in 2013 is an improvement in the measurement precision and derives from switching from an older mass spectrometer (Agilent 5973) to a newer model (Agilent 5975).

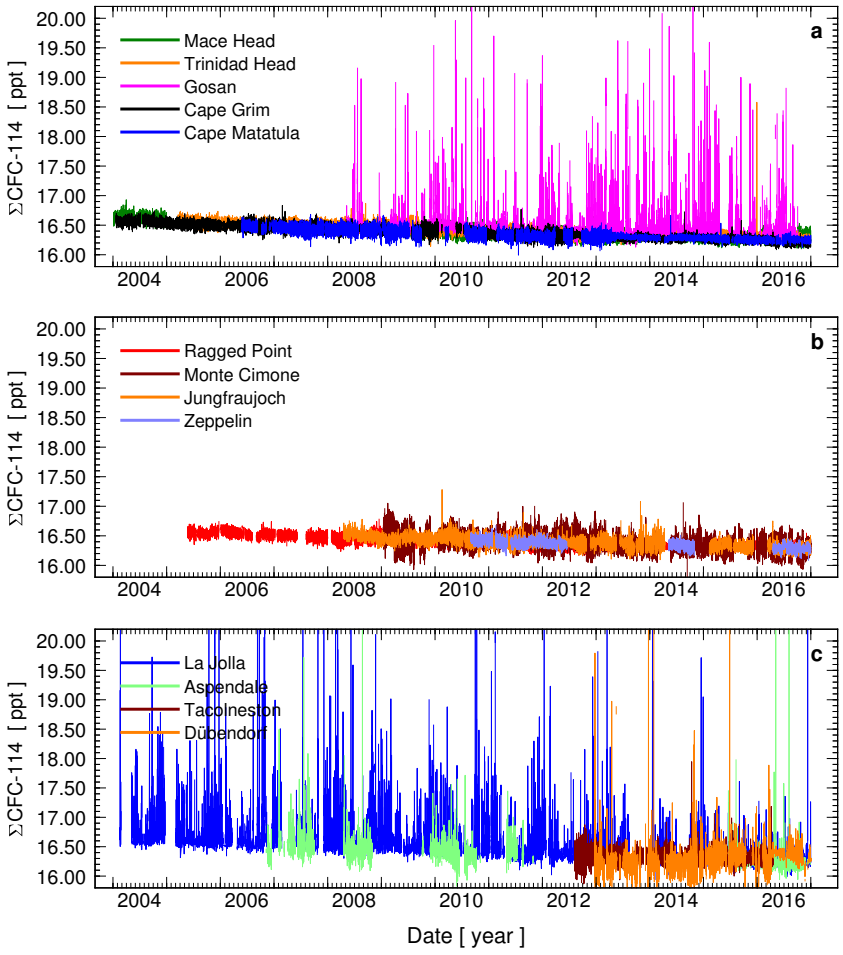

Figure S8. High-resolution (2-hourly) data sets for ΣCFC-114 for nine field (panels a and b) and 4 urban sites (panel c). Gosan is the only field site with significant pollution events recorded. Shangdianzi ΣCFC-114 measurements suffer from a n-butane interference and hence are not further used here. ΣCFC-114 at Monte Cimone before 2009 was measured with poorer precision and larger propagation uncertainties, and is omitted from this plot to avoid obscuring the general interpretation of the records. The urban sites show infrequent pollution events except for La Jolla, where large pollution signals are recorded. At Dübendorf, ΣCFC-114 is depleted in the presence of elevated n-butane mole fractions (see S-4.6). Measurements started at various times at the sites and some had longer interruptions.

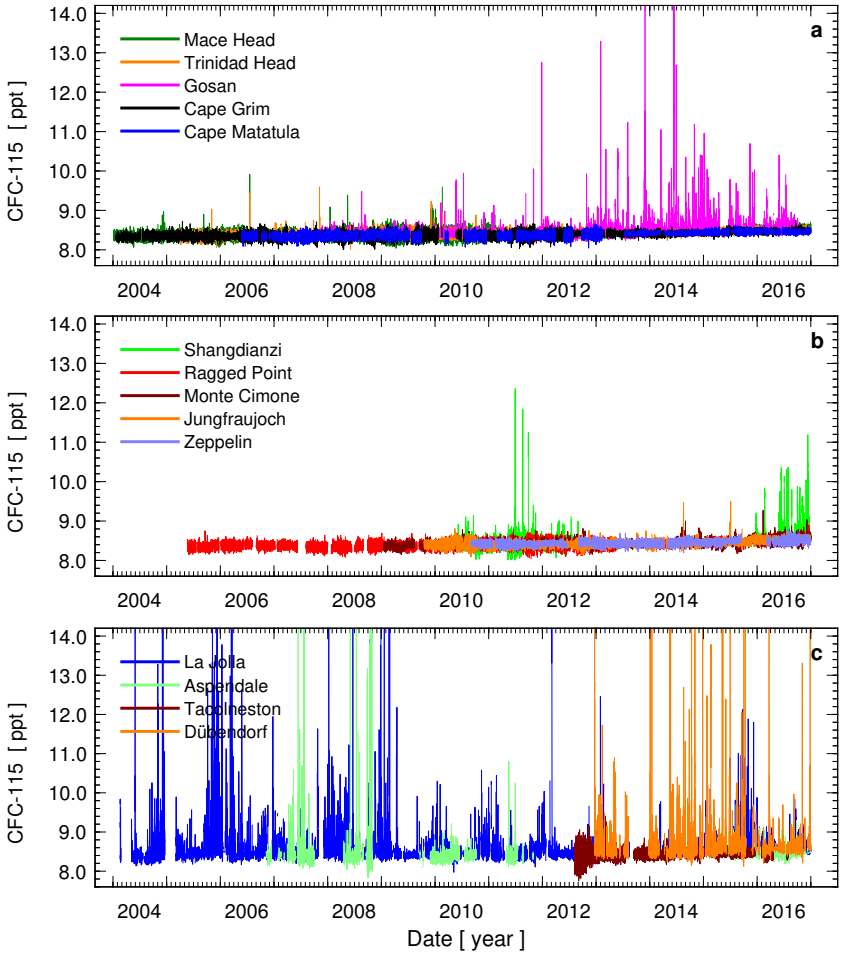

Figure S9. High-resolution (2-hourly) data sets for CFC-115 for ten field (panels a and b) and 4 urban sites (panel c). Gosan and Shangdianzi are the only field sites with significant pollution events recorded. CFC-115 at Monte Cimone before 2009 was measured with poorer precision and is omitted from this plot to avoid obscuring the general interpretation of the records. The urban sites show some CFC-115 sources still present in their footprints for La Jolla, Dubendorf, and the earlier part for Aspendale, but an absence of CFC-115 emissions in the footprint for Tacolneston.

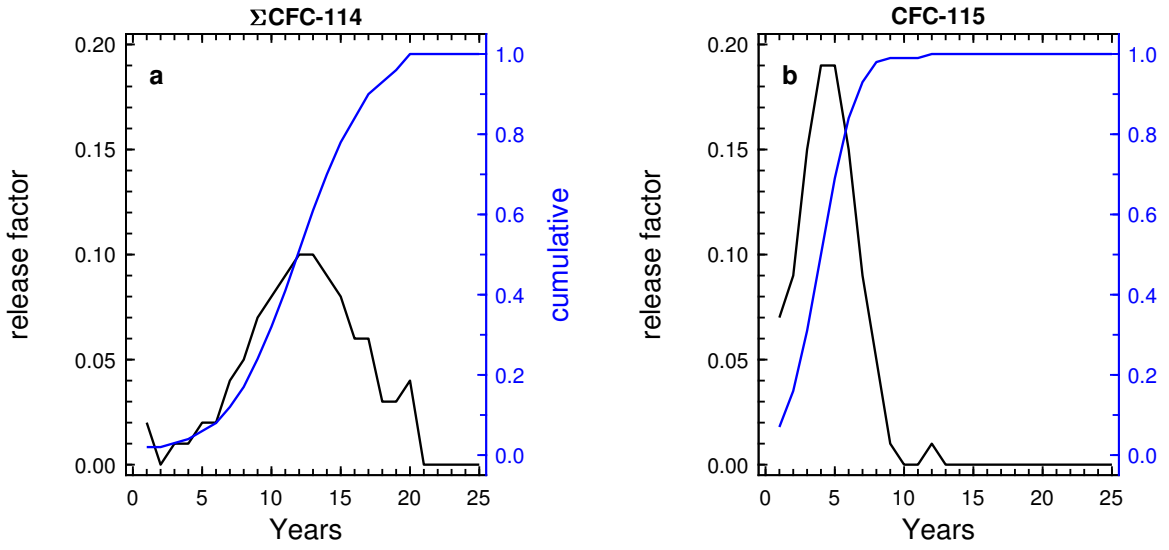

Figure S10. Emission functions for "long-term" release categories for ΣCFC-114 (a) and CFC-115 (b).

emissions were set at 1% from production and 0.3% from distribution processes and occur immediately (Fisher and Midgley, 1993).

Principal uses of these CFCs are in refrigeration: ΣCFC-114 was used on its own in building and nautical air conditioning, CFC-115 was mixed with HCFC-22 as R502 in industrial and commercial refrigeration and cold stores. The differing uses result in different emissions patterns used in the vintaging model to calculate annual emissions. These patterns were derived from a survey of the fluorocarbon producing industry as described in Fisher and Midgley (1993). For ΣCFC-114, emission of the whole charge from the refrigeration equipment takes up to 20 years with a maximum rate in the 12th year following charging (Fig. S10a). In the case of CFC-115 in R502, emissions occur earlier in the life cycle and the whole charge is released within ten years with maximum rates in years 4 and 5 (Fig. S10b).

CFC-115 is not used as a chemical feedstock but, in recent years, ΣCFC-114 has been used to produce HFC-134a. The average quantity of all CFCs consumed in chemical feedstock over the past decade is 200 kt yr^{-1} but this will include all other CFCs (particularly CFC-12) (UNEP, 2016) and so represents an unrealistic upper boundary for ΣCFC-114. Fugitive emissions from the feedstock use of fluorocarbons are now considered to be about 0.1% (0.07 to 0.11%) of the quantity, as estimated by the European Environment Agency (EEA) (EEA, 2016a, b), and so the maximum additional quantity of ΣCFC-114 emitted from feedstock use is 200 t yr^{-1}. However, this value is so uncertain that it has not been included in the results. The emission functions were applied to the categorized sales reported in AFEAS (2007) using the vintaging model described in Gamlen et al. (1986), with the results shown in Table S9. These data were used to calculate the atmospheric mixing ratio scenarios given in Daniel and Velders (2007), and in Velders and Daniel (2014). Here we use them as prior in the 12-box model and compare them to the top-down emission estimates.

The AFEAS data collection for CFCs ceased in 2003 because CFC production by the reporting companies had fallen to 2% of its peak value. At that time, production of ΣCFC-114 and CFC-115 by reporting companies for emissive uses in non-Article 5 countries had fallen to zero and there was no evidence to show significant additional production and use in Article 5 countries, such as India and China. However, an allowance was made in the scenario for continuing use in emissive applications, on a reducing scale for ΣCFC-114 and at a constant value for CFC-115.

S-5.1 Prior for CFC-13

For CFC-13 no bottom-up inventory-based emissions exist. However a prior for emissions is needed by the 12-box model that we use in our analysis. To derive a prior we assume that production, use, and release of CFC-13 in the past was similar to CFC-115 but scaled to smaller quantities. Under this assumption, and given that both compounds have very long lifetimes, it would be easiest to derive CFC-13 bottom up emissions by scaling down the CFC-115 AFEAS bottom-up data using the CFC-13/CFC-115 abundance ratios in the atmosphere (currently 3/8). However such an approach uses atmospheric observations and is somewhat a circular conclusion, which we try to avoid. The very crude approach we have taken is still based on the above assumption of similarities to CFC-115, however we are comparing production data rather than atmospheric abundances. For CFC-115 we take the AFEAS production data (Table S9). As a surrogate for CFC-13 production we use the UNEP Montreal Protocol production data for Protocol Annex B Group I (http://ozone.unep.org/en/data-reporting/data-centre). CFC-13 is the only compound of this group that had a significant commercial use (A. McCulloch, pers. comm 2017). We have extracted the individual countries' contributions and summed these after eliminating the "negative productions" (destructions). The resulting CFC-13 (BI group) production is shown in Fig. S11 along with AFEAS production data for ΣCFC-114 and CFC-115. CFC-13 data are only available starting 1989. For a very rough match with CFC-115 over this period, the CFC-13 (BI group) production needs multiplication by factor 7. To obtain a full CFC-113 prior for emissions we take the CFC-115 emissions shown in Table S9 and divide these by this factor.

S-6 Details on Firn Air Analysis

Firn air measurement and model results are given in the separate Supplement Table S1. Note that in the inversions, a minimum value for the firn measurement uncertainties is chosen, and used whenever the measurement precisions listed in this table are lower than the minimum value. The measurement precisions are sometimes very low and it appears unrealistic to try to fit them to that low level with an imperfect firn model and atmospheric transport model. Instead of the measurement precisions, lower thresholds are chosen of 0.04 ppt for CFC-13, 0.15 ppt for ΣCFC-114, and 0.20 ppt for CFC-115. Each firn measurement is assigned an integer flag 1–4 that indicates whether a chromatographic peak exists and is clearly defined as such, and to what extent it exceeds the noise levels. Further description of the flag values and detection limits are given in Table S1.

In Table S1 we also list ranges for the modeled mole fractions. These minimum (mod-min) and maximum (mod-max) values are from the range generated by the inversion, repeated with combinations of Green's functions from the ensemble, so reflect the influence of firn model errors (but not data errors) on the modeled concentration at the measurement depth.

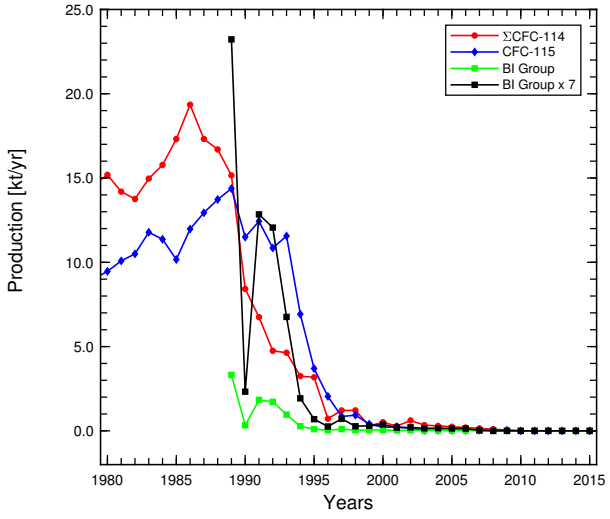

Figure S11. Determination of a prior for CFC-13. Global production data for Montreal Protocol Annex B Group I compounds (of which CFC-13 is the main representative) are compared to those for CFC-115 and a scaling factor of 7 was estimated. This scaling factor was applied to the CFC-115 AFEAS emissions to derive CFC-13 bottom up emissions.

Figures S12, S13 and S14 show Green's functions and some sensitivity analysis for the CSIRO inversions. The top panels show the Green's functions, one line for each firn air sample, that are generated by the firn model and used in the inversions to represent the distribution of ages of the CFCs in air at each measurement depth. There is a great deal of overlap of the Green's functions at different sites and measurement depths. They are shown with dashed lines when they correspond to depths with mole fraction that is zero or below the detection limit. Note that there are two sample flasks for 52 m at DSSW20K, one showing zero mole fraction for CFC-13 (flag value is 4 indicating no sign of a peak), and one with non-zero mole fraction (flag value of 3 indicating that there may be a peak). It is difficult to tell whether the CFC-13 mole fraction at this depth in the firn is zero or not. The recent edge of the CFC-13 Green's function for this depth is older than the recent edge of the 119.87 m South Pole CFC-13 Greens function that has a zero mole fraction (flag=4). Non-zero mole fraction for 52 m DSSW20K seems inconsistent with the South Pole measurement. However, we are comparing measurements at about the level of detection. The DSSW20K sample may have zero mole fraction, or it may have small but non-zero mole fraction and the amount of air in the South Pole sample from the 1950s–60s with low mole fraction is such a small proportion of the entire sample that no CFC-13 is detected. Or there may be errors in the edges of one or the other of the Green's functions from the firn model. The difference it makes to the CSIRO inversion, when we consider only zero mole fraction at 52 m DSSW20K, or with both the zero and non-zero values, is within the uncertainties in emissions. It is also to be noted that for CFC-115, two of three sample flasks for the 52 m depth show zero mole fraction while one is non-zero. Also, the South Pole CFC-115 is non-zero.

The middle panels show the CSIRO inversion results calculated by excluding measurements from one dataset at a time (for the firn sites and the CG and NH archive records, but not the in situ measurements), to test the influence of individual

datasets on the reconstructed emissions. The double peaked structure of the ΣCFC-114 emissions is a robust feature, occurring in all solutions of the CSIRO inversion with one dataset excluded (and indeed in all solutions of the CSIRO inversion in the development of this work). There is some uncertainty in the timing and magnitude of the first peak (with a range of about 5 years on the timing and about 3 kt yr^{-1} on the magnitude of the first peak), with the CGAA suggesting an earlier peak (without CGAA the peak moves later) and NEEM-08 suggesting a later peak. Results for the other CFCs do not vary much as datasets are excluded from the inversion. The bottom panels in Figures S12, S13 and S14 show emissions from the CSIRO inversion for different values of the regularization parameter α that is used to weight a term in the cost function that depends on the year-to-year changes in emissions, relative to the model-data mismatch (Trudinger et al., 2016). Regularization is required because the inversion for annual emissions from firn data is ill-conditioned, and it is used in the CSIRO model to avoid solutions with large, unrealistic oscillations.

S-7 CFC-13 Emissions From An Aluminum Smelter

Penkett et al. (1981) and Harnisch (1997) found elevated CFC-13 in the exhausts of aluminum smelters. Based on these findings and the current efforts to provide a CFC-13 global history, we have re-investigated the measurement results from a study on an Australian aluminum smelter (Fraser et al., 2013). A careful inspection of the data has shown that CFC-13 emissions were overlooked and the false conclusion of their absence was drawn. The samples had been collected from the Kurri Kurri smelter (New South Wales) in 2009 using time-integrated stack sampling. The individual CFC-13 measurement results (corrected for a background atmospheric concentration of 2.9 ppt) were as follows (compare with Table 3 in Fraser et al. (2013): L1N(E): 0.046 ppb (parts-per-billion); L2N(E): 0.045 ppb; L2S(E): 0.127 ppb; L2N(R): -0.001 ppb; Mass emissions (compare with Table 4 in Fraser et al. (2013)) over the sampling periods were: L1NE: 13.9 kg; L2NE: 18.5 kg L2SE: 46.1 kg; L2NR: -1.8 kg; L2N(E+R): 16.7 kg. From this, emissions of L1N(E+R) = 12.5 kg and L2S(E+R) = 41.6 kg were calculated. The corresponding emission factors in g CFC-13/tonne aluminum (see Table 5 in Fraser et al. (2013) were: L2N: 0.016; L1N: 0.014; L2S: 0.044; This resulted in an average emissions factor of 0.025 with a 1σ std. dev of 0.017; This emission factor is significantly smaller compared to the CF_4 and PFC-116 emission factors found in that study but of a similar magnitude as that of PFC-218. By comparison, the emissions factors found by Harnisch (1997) were significantly larger for all three PFCs and also for CFC-13, for which he found 10 g/tonne of aluminum.

S-8 Regional Scale Sources

Details on the regional scale inversion method used for East Asian CFC emissions can be found in Henne et al. (2016). The method optimizes the spatial distribution of temporally constant CFC emissions so that simulated and observed atmospheric concentrations of the compound agree best. Simulated concentrations consist of a directly simulated regional contribution and a baseline contribution. The regional contribution results from emissions taken up during the 10-day transport time of the FLEXPART backward simulation. This is further split into contributions from within and outside the inversion domain

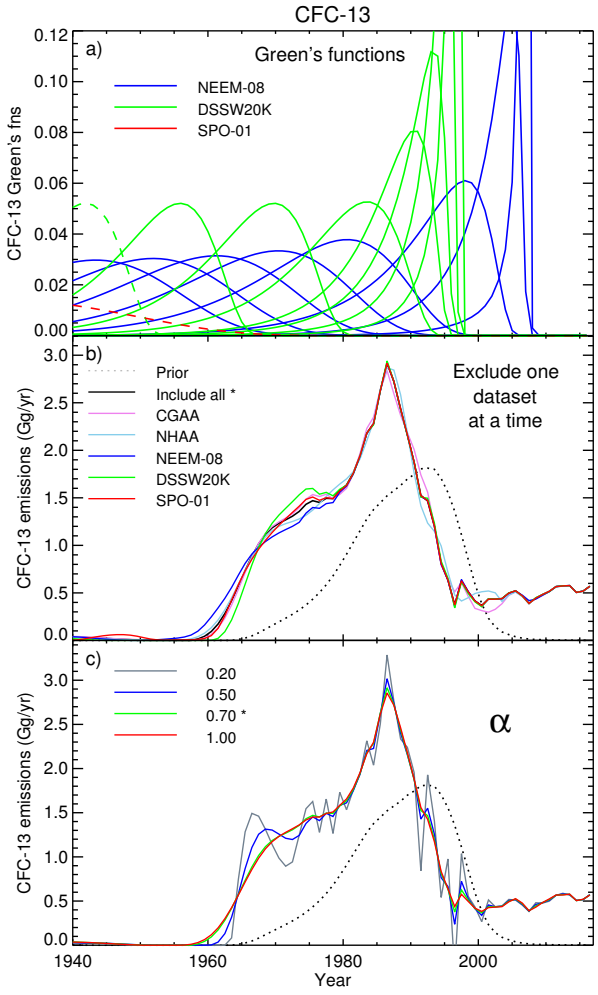

Figure S12. Green's functions from the CSIRO firn air model (a) and sensitivity analysis for results from the CSIRO inversion (panels b and c) for CFC-13. There is one Green's function for each measurement depth, shown with a dashed line when it corresponds to mole fraction measurements that are zero or below the detection limit. Panel b shows results from the CSIRO inversion with firn and archive datasets excluded one at a time. Panel c shows results from the CSIRO inversion with different values of the regularization parameter α. In panels b and c, prior emissions are shown by dotted lines, and our standard case is indicated in the legend by an asterisk.

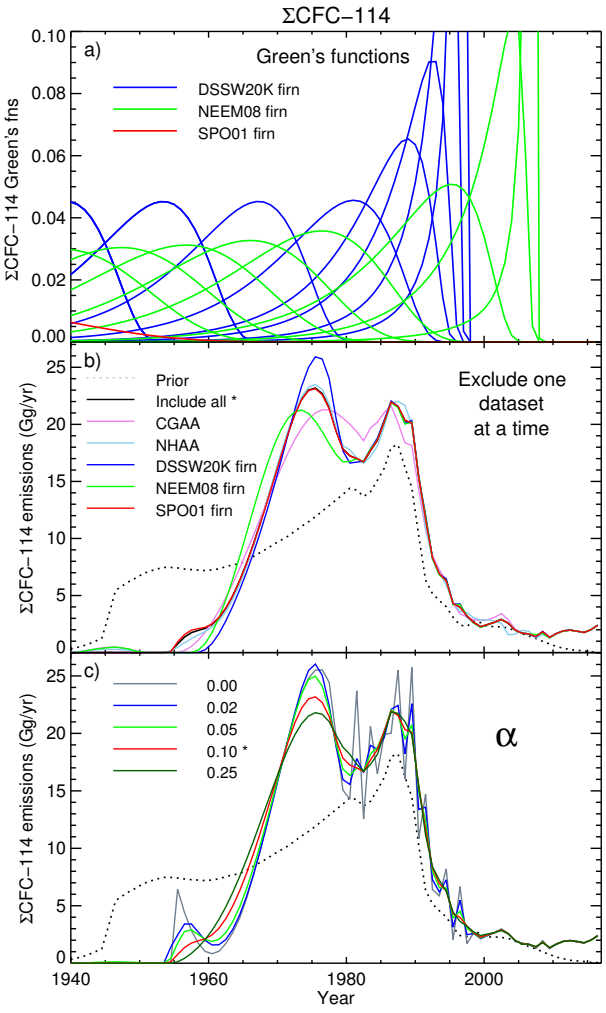

Figure S13. Green's functions from the CSIRO firn air model (a) and sensitivity analysis for results from the CSIRO inversion (panels b and c) for ΣCFC-114, as in Figure S12.

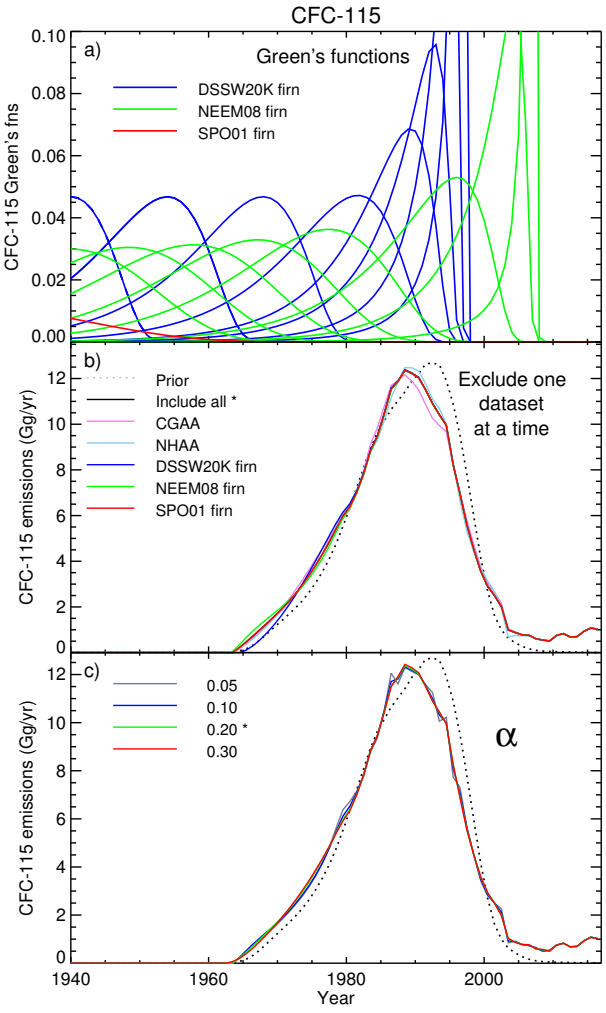

Figure S14. Green's functions from the CSIRO firn air model (a) and sensitivity analysis for results from the CSIRO inversion (panels b and c) for CFC-115, as in Figure S12.

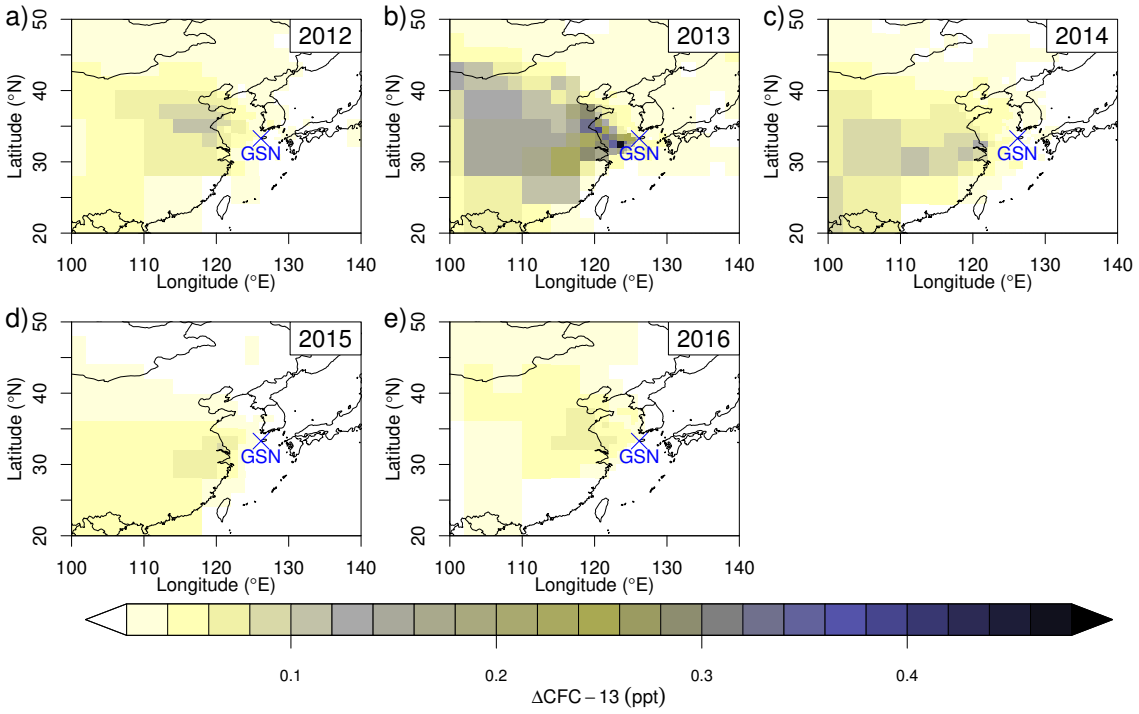

Figure S15. Potential source locations of CFC-13 in Eastern Asia as derived from above-baseline observations at Gosan (blue cross) and FLEXPART simulated source sensitivities. The values depicted represent a weighted average of the observed above-baseline observations (units ppt) using the spatial distribution of the source sensitivities as weights.

depicted in Fig. S15–S17. Only emissions within the inversion domain are optimized, whereas those outside remain at their prior level. In addition, a statistical baseline fit (Ruckstuhl et al., 2012) was applied to the observations and the resulting baseline was considered as the baseline contribution of the simulation. All observations were aggregated to 3-hourly bins for which FLEXPART simulations were carried out. All valid observations were used in the inversion, no additional filtering by time-of-day or wind direction was applied. The inversion grid was constructed following the average simulated source sensitivity for the site Gosan with smaller grid cells where source sensitivities were larger and larger grid cells where source sensitivities were smaller. This resulted in a total of 500 inversion grid cells for the year 2014, which can be compared to about 2200 3-hourly observations for the same period. Next to emissions in the reduced inversion grid also the smooth baseline was added to the state vector of the Bayesian inversion. This was done in the form of 5-daily baseline scaling factors, adding another 55 elements to optimize by the inversion.

Within the Bayesian inversion, complete covariance matrices for the prior and data-mismatch uncertainties were used. This included the treatment of covariance in the observations with a temporal correlation length of 0.25 days, which was calculated from an exponential fit to the empirical auto-correlation of the prior model residuals. Furthermore, the relative total uncertainty

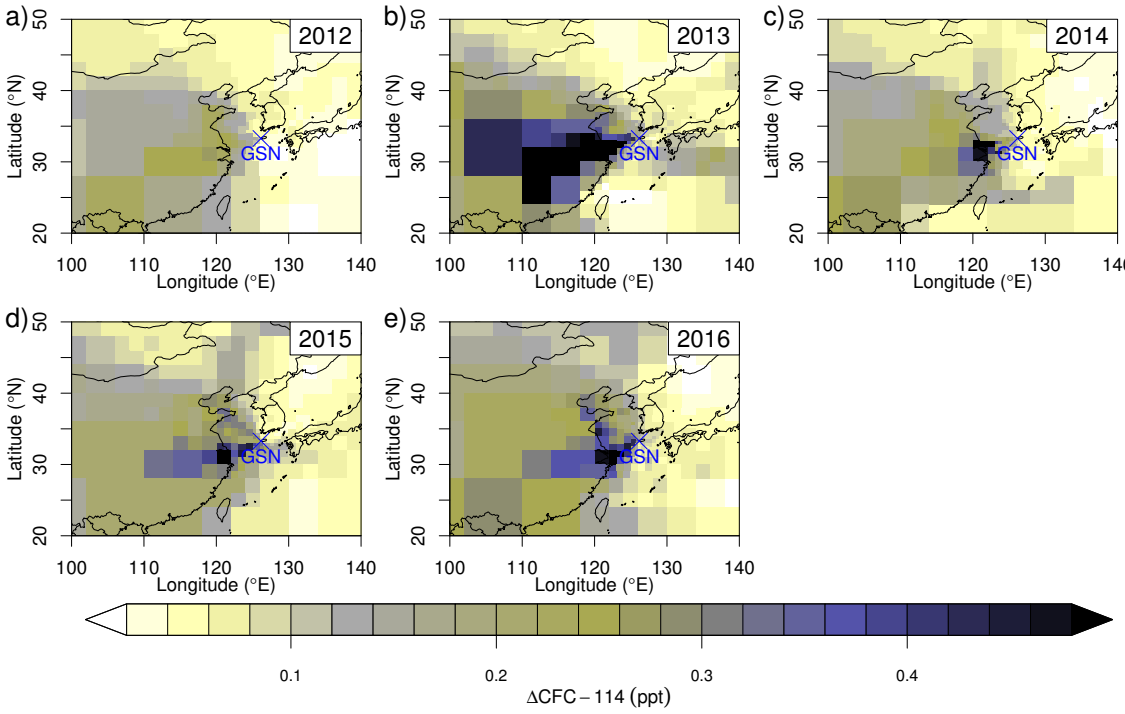

Figure S16. Potential source locations of ΣCFC-114 in Eastern Asia as derived from above-baseline observations at Gosan (blue cross) and FLEXPART simulated source sensitivities. The values depicted represent a weighted average of the observed above-baseline observations (units ppt) using the spatial distribution of the source sensitivities as weights.

σ_E and spatial correlation length scale L of the prior emissions, the absolute uncertainty σ_b and temporal correlation length scale τ_b of the prior baseline, and two parameters describing the absolute and relative (to simulated sensitivity) data-mismatch uncertainty, σ_{min} and σ_{srr}, were obtained from a log-likelihood (LLH) maximum search (Michalak et al., 2005; Henne et al., 2016) using the observations/simulations of the year 2014 (Table S12).

To illustrate the performance of the regional scale inversion system the time series of observed and simulated (prior and posterior) CFC-115 at Gosan is shown in Figure S18. The observed evolution of the CFC-115 signal at Gosan was characterized by a series of large pollution events that overshadow most other variability and trend in the time series. The prior simulation (dark red) is not able to reproduce any of the observed peaks at all, neither in timing nor in magnitude. In contrast, using the posterior emissions obtained by the inversion, the timing of many of the observed peaks can be reproduced by the model (dark blue). Only a few simulated peaks occurred at times when no peaks were observed.

This model performance improvement can also be seen in time-series comparison statistics for all compounds and all years, indicated by increased posterior correlation coefficients and reduced root mean square errors (Figures S19, S20, S21). The improved correlation coefficient was mostly achieved through improvements of the above-baseline signal, the part of the

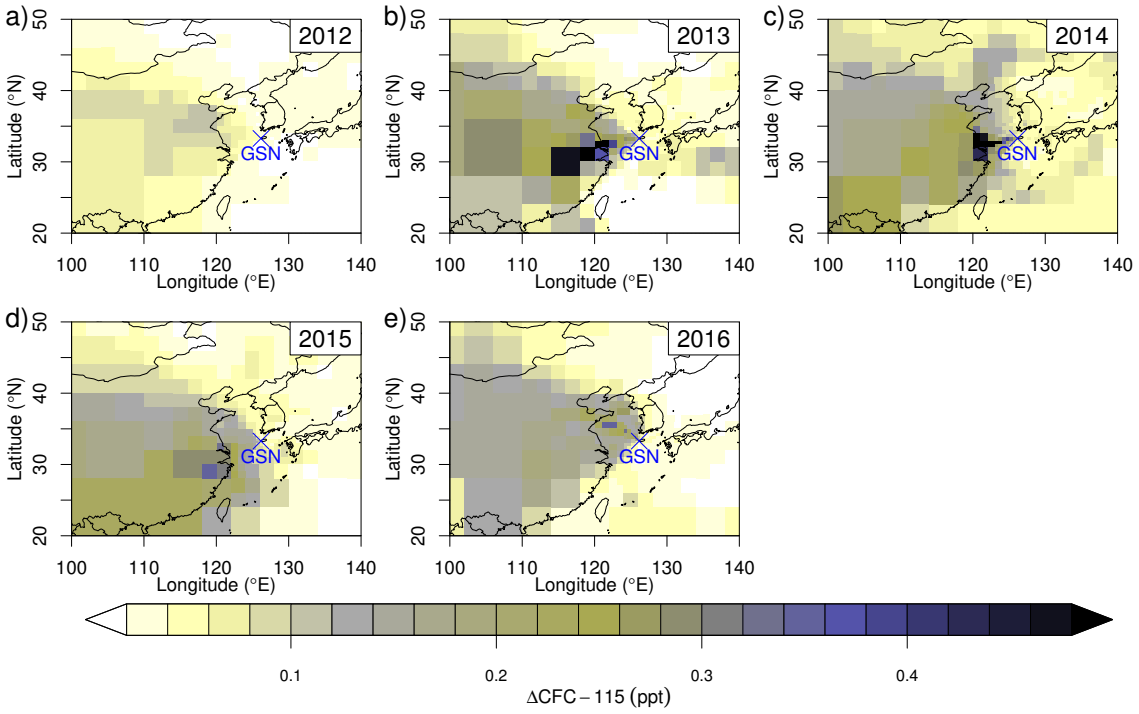

Figure S17. Potential source locations of CFC-115 in Eastern Asia as derived from above-baseline observations at Gosan (blue cross) and FLEXPART simulated source sensitivities. The values depicted represent a weighted average of the observed above-baseline observations (units ppt) using the spatial distribution of the source sensitivities as weights.

simulated time-series that is due to recent emission uptake, and not through adjustments of the baseline itself. In general the performance and its improvement was larger for ΣCFC-114 and CFC-115 than for CFC-13, indicating the difficulties of the transport and inversion model to correctly identify the CFC-13 emissions. There is also considerable year-to-year variability in the performance with the tendency of larger correlation coefficients for years with larger posterior emissions. For ΣCFC-114 and CFC-115 and considering the strongly skewed character of the probability density distribution of the observations (few large pollution peaks) and the lack of any prior knowledge of the location and strength of large sources, these performance statistics give credibility to the obtained posterior emissions for these compounds.

The choice of the magnitude of the prior emission was tested by running additional sensitivity inversions with 50emissions. The influence on the a-posteriori emissions was small compared to the a-posteriori uncertainty estimate.

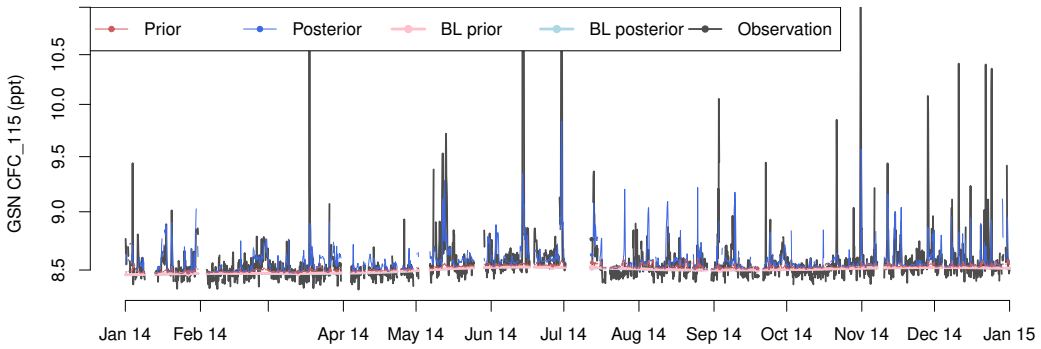

Figure S18. Observed and simulated CFC-115 time series at Gosan for the year 2014.

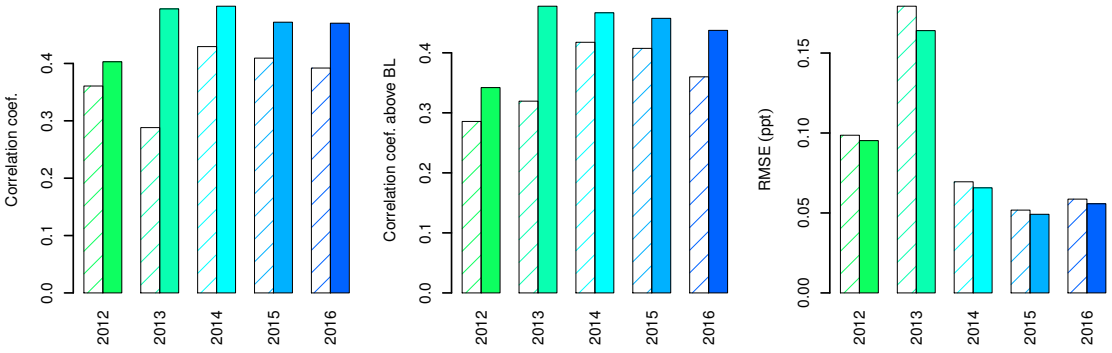

Figure S19. Regional scale model skills as evaluated against Gosan CFC-13 observations. Prior performance is shown as shaded bars and posterior performance as filled bars. a) Correlation coefficient for the complete time series, b) correlation coefficient for the regional (above baseline) part of the time series, c) root mean square error.

Table S12. Overview of uncertainty covariance settings used for the Asian regional inversion as derived from LLH optimization. For details see text.

Compound	σ_E (%)	L (km)	σ_b (ppt)	τ_b (days)	σ_{min} (ppt)	σ_{srr} (-)
CFC-13	39	236	0.007	16	0.03	2.1
ΣCFC-114	90	135	0.007	16	0.10	2.5
CFC-115	340	70	0.008	16	0.1	5.8

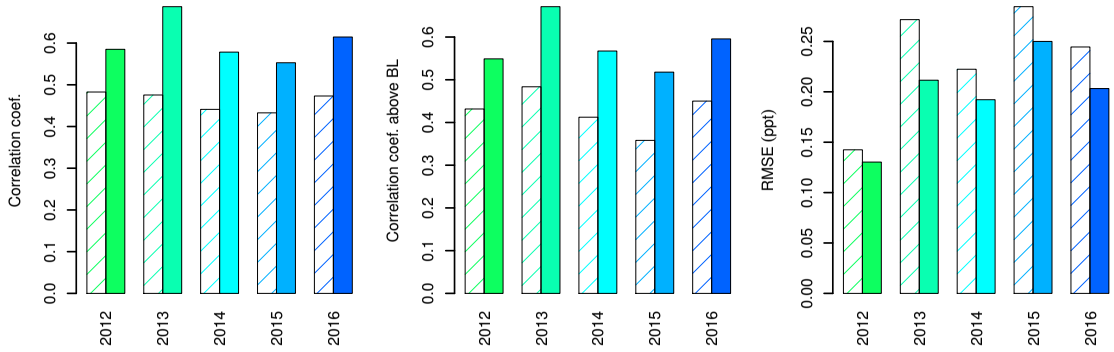

Figure S20. Regional scale model skills as evaluated against Gosan ΣCFC-114 observations. Prior performance is shown as shaded bars and posterior performance as filled bars. a) Correlation coefficient for the complete time series, b) correlation coefficient for the regional (above baseline) part of the time series, c) root mean square error.

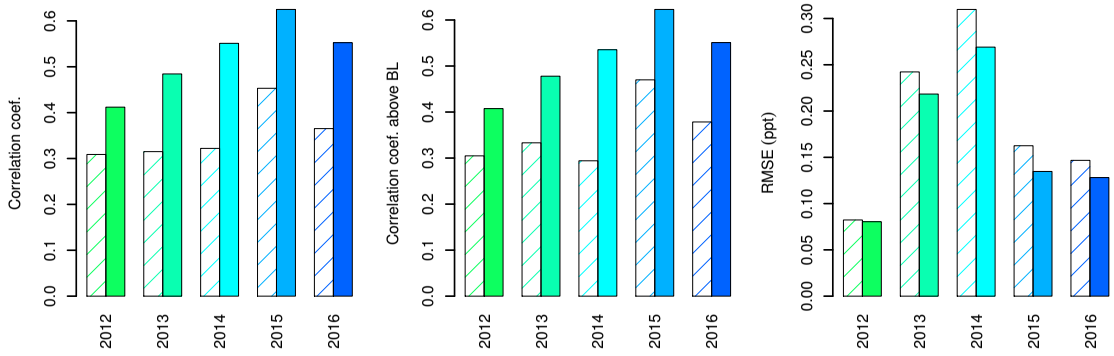

Figure S21. Regional scale model skills as evaluated against Gosan CFC-115 observations. Prior performance is shown as shaded bars and posterior performance as filled bars. a) Correlation coefficient for the complete time series, b) correlation coefficient for the regional (above baseline) part of the time series, c) root mean square error.

References

Daniel, J. S. and Velders, G. J. M.: Halocarbon Scenarios, Ozone Depletion Potentials, and Global Warming Potentials Chapter 8, in: Scientific Assessment of Ozone Depletion: 2006, Global Ozone Research and Monitoring Project—Report No. 50, p. 572, World Meteorological Organization, Geneva, Switzerland, 2007.

EEA: Production and consumption of ozone-depleting substances, http://www.eea.europa.eu/data-and-maps/indicators/production-and-consumption-of-o 2016a.

EEA: Ozone-depleting Substances 2015, Tech. Rep. 19/2016, European Environment Agency, 2016b.

Fisher, D. A. and Midgley, P. M.: The production and release to the atmosphere of CFCs 113, 114 and 115, Atmos. Environ., 27A, 271–276, doi:10.1016/0960-1686(93)90357-5, 1993.

Fraser, P., Steele, P., and Cooksey, M.: PFC and carbon dioxide emissions from an Australian aluminium smelter using time-integrated stack sampling and GC-MS, GC-FID analysis, in: Light Metals 2013, edited by Sadler, B. A., pp. 871–876, John Wiley & Sons, Inc., Hoboken, NJ, USA, doi:10.1002/9781118663189.ch148, 2013.

Gamlen, P. H., Lane, B. C., Midgley, P. M., and Steed, J. M.: The production and release to the atmosphere of CCl_3F and CCl_2F_2 (chlorofluorocarbons CFC-11 and CFC-12), Atmos. Environ., 20, 1077–1085, 1986.

Harnisch, J.: Die Globalen Atmosphärischen Haushalte der Spurengase Tetrafluormethan (CF_4) und Hexafluorethan (C_2F_6), Ph.D. Thesis, University of Gottingen, 1997.

Henne, S., Brunner, D., Oney, B., Leuenberger, M., Eugster, W., Bamberger, I., Meinhardt, F., Steinbacher, M., and Emmenegger, L.: Validation of the Swiss methane emission inventory by atmospheric observations and inverse modelling, Atmos. Chem. Phys., 16, 3683–3710, doi:10.5194/acp-16-3683-2016, 2016.

Ivy, D. J., Arnold, T., Harth, C. M., Steele, L. P., Mühle, J., Rigby, M., Salameh, P. K., Leist, M., Krummel, P. B., Fraser, P. J., Weiss, R. F., and Prinn, R. G.: Atmospheric histories and growth trends of C_4F_{10}, C_5F_{12}, C_6F_{14}, C_7F_{16} and C_8F_{18}, Atmos. Chem. Phys., 12, 4313–4325, doi:10.5194/acp-12-4313/2012, 2012.

Laube, J. C., Mohd Hanif, N., Martinerie, P., Gallacher, E., Fraser, P. J., Langenfelds, R., Brenninkmeijer, C. A. M., Schwander, J., Witrant, E., Wang, J.-L., Ou-Yang, C.-F., Gooch, L. J., Reeves, C. E., Sturges, W. T., and Oram, D. E.: Tropospheric observations of CFC-114 and CFC-114a with a focus on long-term trends and emissions, Atmos. Chem. Phys., pp. 15 347–15 358, doi:10.5194/acp-16-15347-2016, http://www.atmos-chem-phys.net/16/15347/2016/, 2016.

McCulloch, A., Midgley, P. M., and Fisher, D. A.: Distribution of emissions of chlorofluorocarbons (CFCs) 11, 12, 113, 114, 115 among reporting and non-reporting countries in 1986, Atmos. Environ., 28, 2567–2582, doi:10.1016/1352-2310(94)90431-6, 1994.

Michalak, A. M., Hirsch, A., Bruhwiler, L., Gurney, K. R., Peters, W., and Tans, P. P.: Maximum likelihood estimation of covariance parameters for Bayesian atmospheric trace gas surface flux inversions, J. Geophys. Res. Atmos., 110, D24 107, doi:10.1029/2005JD005970, 2005.

Miller, B. R., Rigby, M., Kuijpers, L. J. M., Krummel, P. B., Steele, L. P., Leist, M., Fraser, P. J., McCulloch, A., Harth, C., Salameh, P., Mühle, J., Weiss, R. F., Prinn, R. G., Wang, R. H. J., O'Doherty, S., Greally, B. R., and Simmonds, P. G.: CHF_3 (HFC-23) emission trend response to $CHClF_2$ (HCFC-22) production and recent CHF_3 emission abatement measures, Atmos. Chem. Phys., 10, 7875–7890, doi:10.5194/acp-10-7875-2010, 2010.

Oram, D. E.: Trends of Long-Lived Anthropogenic Halocarbons in the Southern Hemisphere and Model Calculation of Global Emissions, Ph.D. Thesis, University of East Anglia, U.K., 1999.

Penkett, S. A., Prosser, N. J. D., Rasmussen, R. A., and Khalil, M. A. K.: Atmospheric measurements of CF_4 and other fluorocarbons containing the CF_3 grouping, J. Geophys. Res., 86, 5172–5178, doi:10.1029/JC086iC06p05172, 1981.

Ruckstuhl, A. F., Henne, S., Reimann, S., Steinbacher, M., Vollmer, M. K., O'Doherty, S., Buchmann, B., and Hueglin, C.: Robust extraction of baseline signal of atmospheric trace species using local regression, Atmos. Meas. Tech., 5, 2613–2624, doi:10.5194/amt-5-2613-2012, 2012.

Sturrock, G. A., Etheridge, D. M., Trudinger, C. M., Fraser, P. J., and Smith, A. M.: Atmospheric histories of halocarbons from analysis of Antarctic firn air: Major Montreal Protocol species, J. Geophys. Res., 107, 4765, doi:10.1029/2002JD002548, 2002.

Trudinger, C. M., Enting, I. G., Rayner, P. J., Etheridge, D. M., Buizert, C., Rubino, M., Krummel, P. B., and Blunier, T.: How well do different tracers constrain the firn diffusivity profile?, Atmos. Chem. Phys., 13, doi:10.5194/acp-13-1485-2013, 2013.

Trudinger, C. M., Fraser, P. J., Etheridge, D. M., Sturges, W. T., Vollmer, M. K., Rigby, M., Martinierie, P., Mühle, J. Worton, D. R., Krummel, P. B., Steele, L. P., Miller, B. R., Laube, J., Mani, F., Rayner, P. J., Harth, C. M., Witrant, E., Blunier, T., Schwander, J., O'Doherty, S., and Battle, M.: Atmospheric abundance and global emissions of perfluorocarbons CF_4, C_2F_6 and C_3F_8 since 1800 inferred from ice core, firn, air archive and in situ measurements, Atmos. Chem. Phys., 16, 11 733–11 754, doi:10.5194/acp-16-11733-2016, 2016.

UNEP: Information provided by parties in accordance with Articles 7 and 9 of the Montreal Protocol on Substances that Deplete the Ozone Layer, http://conf.montreal-protocol.org/meeting/mop/mop-28/presession/English/MOP-28-9-IMPCOM-57-2E.pdf, 2016.

Velders, G. J. M. and Daniel, J. S.: Uncertainty analysis of projections of ozone-depleting substances: mixing ratios, EESC, ODPs, and GWPs, Atmos. Chem. Phys., 14, 2757–2776, doi:10.5194/acp-14-2757-2014, http://www.atmos-chem-phys.net/14/2757/2014/, 2014.